Rangeland Ecology & Management 69 (2016) 95–107

Contents lists available at ScienceDirect

Rangeland Ecology & Management

journal homepage: http://www.elsevier.com/locate/rama

Editor's Choice Research Article

Spatially Explicit Rangeland Erosion Monitoring Using High-Resolution Digital Aerial Imagery☆,☆☆

Jeffrey K. Gillan [a,*], Jason W. Karl [b], Nichole N. Barger [c], Ahmed Elaksher [d], Michael C. Duniway [e]

[a] Geospatial Specialist, US Department of Agriculture—Agricultural Research Service Jornada Experimental Range, New Mexico State University, Las Cruces, NM 88003–8003, USA
[b] Research Ecologist, US Department of Agriculture—Agricultural Research Service Jornada Experimental Range, New Mexico State University, Las Cruces, NM 88003–8003, USA
[c] Assistant Professor, University of Colorado at Boulder, Department of Ecology and Evolutionary Biology, Boulder, CO 80309, USA
[d] Assistant Professor, New Mexico State University, Department of Engineering Technology and Surveying Engineering, Las Cruces, NM 88003–8001, USA
[e] Research Ecologist, U.S. Geological Survey, Southwest Biological Science Center, Moab, UT 84532, USA

ARTICLE INFO

Article history:
Received 27 October 2014
Accepted 26 October 2015

Keywords:
change detection
digital elevation model
photogrammetry
rangeland monitoring
remote sensing
soil erosion

ABSTRACT

Nearly all of the ecosystem services supported by rangelands, including production of livestock forage, carbon sequestration, and provisioning of clean water, are negatively impacted by soil erosion. Accordingly, monitoring the severity, spatial extent, and rate of soil erosion is essential for long-term sustainable management. Traditional field-based methods of monitoring erosion (sediment traps, erosion pins, and bridges) can be labor intensive and therefore are generally limited in spatial intensity and/or extent. There is a growing effort to monitor natural resources at broad scales, which is driving the need for new soil erosion monitoring tools. One remote-sensing technique that can be used to monitor soil movement is a time series of digital elevation models (DEMs) created using aerial photogrammetry methods. By geographically coregistering the DEMs and subtracting one surface from the other, an estimate of soil elevation change can be created. Such analysis enables spatially explicit quantification and visualization of net soil movement including erosion, deposition, and redistribution. We constructed DEMs (12-cm ground sampling distance) on the basis of aerial photography immediately before and 1 year after a vegetation removal treatment on a 31-ha Piñon-Juniper woodland in southeastern Utah to evaluate the use of aerial photography in detecting soil surface change. On average, we were able to detect surface elevation change of $\pm 8-9$cm and greater, which was sufficient for the large amount of soil movement exhibited on the study area. Detecting more subtle soil erosion could be achieved using the same technique with higher-resolution imagery from lower-flying aircraft such as unmanned aerial vehicles. DEM differencing and process-focused field methods provided complementary information and a more complete assessment of soil loss and movement than any single technique alone. Photogrammetric DEM differencing could be used as a technique to quantitatively monitor surface change over time relative to management activities.

Introduction

Soil and site stability are key attributes of assessing the health of arid and semiarid lands (National Research Council, 1994; Pyke et al., 2002) because these lands are susceptible to high rates of wind and water erosion. Erosion results in loss of soil nutrients and organic matter, leaving it less productive (Pimentel and Kounang, 1998; Heng et al., 2010) and vulnerable to transition to undesirable alternate and/or degraded states (Chartier and Rostagno, 2006; Okin, 2008; Kéfi et al., 2010). Nearly all of the ecosystem services supported by rangelands, including production of livestock forage, carbon sequestration, and provisioning of clean water, are negatively impacted by soil erosion (Hassan et al., 2005). Soil loss due to hydrologic processes can reduce water quality in streams and rivers, while wind-blown soil can reduce air quality, damage property, and negatively impact downwind mountain snowpack (National Research Council, 1994; Pimentel et al., 1995; Painter et al., 2010; USDA, 2010). In addition, soil erosion driven by land use and climate plays a large role in desertification (Schlesinger et al., 1990; Peters et al., 2004, 2007). Accordingly, monitoring the severity, spatial extent, and rate of soil erosion is essential for long-term sustainable management of rangelands.

A variety of field techniques have been developed to measure and monitor the rates of erosion and sediment transport. Sediment traps, perhaps the most common method, include passive dust samplers for measuring wind-driven flux (Wilson and Cooke, 1980; Fryrear, 1986) and hillslope or catchment-scale overland flow retainers for measuring water-driven fluxes (silt fences and stock ponds; Loughran, 1989; Robichaud, 2005; Nichols, 2006). From accumulation of sediment in the traps over time, sediment transport rates (e.g., $g \cdot m^{-2} \cdot d^{-1}$) caused

☆ Any use of trade, firm, or product names is for descriptive purposes only and does not imply endorsement by the U.S. Government.

☆☆ This research was supported by a US Dept of Agriculture National Research Initiative—Managed Ecosystems grant to N. N. Barger (Proposal 2008–00776).

* Correspondence: Tel.: +1 575 646 2961; fax: +1 575 646 5889.
E-mail address: jgillan@nmsu.edu (J.K. Gillan).

http://dx.doi.org/10.1016/j.rama.2015.10.012
1550-7424/

by either wind (dust samplers) or water (silt fences, stock ponds) can be estimated. A limitation of these methods is the difficulty of identifying the area from which the sediment originated and where it is going. Determining the source area for dust samplers is not easily done, and typically horizontal flux (not erosion) rates are estimated (Zhang et al., 2011). The potential source area can usually be determined for water-transported sediment, allowing for estimates of fluvial erosion rates (e.g., $t \cdot ha^{-1} \cdot y^{-1}$). However, soil erosion is not evenly distributed across a watershed and pinpointing fluvial erosion sources within catchments is still elusive.

Another suite of field methods allows for estimating the spatial distribution of erosion and deposition by measuring net soil surface change over time. Unlike sediment traps, these techniques can account for the spatial variation of sediment movement to help identify sources and sinks of eroded material. These surface change methods do not measure flux, nor are they typically process specific as they measure the aggregated effect of wind, water, and other disturbances. Commonly used techniques include erosion pins (Fanning, 1994; Sirvent et al., 1997) and erosion bridges (Shakesby, 1993; Wilcox et al., 1996) that measure the subsidence of soil compared with a fixed datum. Soil movement can also be tracked by detecting environmental tracers such as Cesium-137 isotopes (Ritchie and McHenry, 1990; Zapata, 2003).

Net soil movement can also be measured with a time series of ground-based digital elevation models (DEMs). By geographically coregistering the DEMs and subtracting one surface from another, an image of soil elevation change can be created (referred to as DEM differencing throughout the paper). Such analysis enables spatially explicit quantification and visualization of net soil movement. Ground-based DEMs can be made from a few different sources including surveying (Martínez-Casasnovas et al., 2002; Wheaton et al., 2010), terrestrial laser scanning (Perroy et al., 2010; Bremer and Sass, 2012; Schneider et al., 2012), and close-range photogrammetry (Welch et al., 1984; Gessesse et al., 2010; Nouwakpo and Huang, 2012).

The resolution and spatial extent of in situ methods for measuring soil erosion is a function of the labor and time allocated for installation, maintenance, and data collection. Intensive field protocols can quickly become expensive in large monitoring programs (Pellant et al., 1999; Booth and Cox, 2008; Marzolff and Poesen, 2009). As a result, field methods usually cover only plot and hillslope scales (an exception being Nichols, 2006). In addition, sample locations may be inaccessible or difficult to access in vehicles or on foot (Pellant et al., 1999). These factors combined with heterogeneity of soil conditions across landscapes make it difficult to scale up soil erosion measurements to make inferences to catchment and watershed scales.

There is a growing effort to monitor natural resources at broad scales that is driving the need for new soil erosion monitoring tools. Regional and continental scale rangeland monitoring programs such as National Resource Inventory (NRI; Nusser and Goebel, 1997; Herrick et al., 2010) and Bureau of Land Management's Assessment, Inventory, and Monitoring program (Toevs et al., 2011) rely on field measurements from thousands of sample locations to track vegetation and soil characteristics. To reduce costs associated with data collection, efficiencies must be sought. Remote sensing techniques employing high-resolution aerial imagery can increase the extent and efficiency of measuring vegetation attributes in rangelands (Booth et al., 2005, 2006; Duniway et al., 2011; Karl et al., 2012) and could potentially be used for monitoring soil erosion rates.

DEM differencing can also be produced from airborne sensors such as airborne laser scanning (i.e., LiDAR), synthetic aperture radar, and photogrammetry from cameras to cover a larger extent of land compared with field methods. Airborne DEM differencing has been demonstrated to measure topographic change for a variety of applications and environments including gullies (Thomas et al., 1986; Vandaele et al., 1996; DeRose et al., 1998; Betts and DeRose, 1999; Martínez-Casasnovas, 2003; Marzolff and Poesen, 2009; Marzolff et al., 2011; d' Oleire-Oltmanns et al., 2012), riverbeds (Smith et al., 2000; Brasington et al., 2003; Lane et al., 2003; Thoma et al., 2005), sand dunes (Brown and Arbogast, 1999), landslides (Bremer and Sass, 2012; Lucieer et al., 2013), and artificial catchments (Schneider et al., 2011, 2012).

However, little research has been conducted with specific consideration to monitoring large upland rangeland landscapes, an application with unique technical challenges (e.g., inaccessibility, variability in woody and herbaceous vegetation cover). To reduce the costs associated with field visits, a workflow that minimizes the need for field-collected ground control is necessary. Also, the spatial resolution of the imagery needs to be fine scale enough to 1) automatically identify and exclude individual trees and shrubs from the DEMs and 2) detect the subtle topographic changes that can occur on rangelands due to erosional processes (cm scale; Fanning, 1994; Sirvent et al., 1997).

We conducted DEM differencing from high-resolution aerial imagery to test the ability to quantify soil erosion on a 31-ha Piñon-Juniper woodland in southeastern Utah. In 2009, a suite of fuel-reduction vegetation treatments were carried out with the goal of reducing fuel loads while restoring native understory vegetation. The specific objectives of this research were to 1) measure soil movement over the course of a year using photogrammetric DEM differencing, 2) assess the precision of the imagery products and subsequent soil erosion estimates and compare the results to concurrent field measurements of sediment flux, and 3) compare rates of erosion and sediment flux between treatment areas to evaluate DEM differencing as a method for estimating soil erosion following land management activities. We were not, however, trying to determine if the specific treatments were the cause of varying erosion rates. We discuss the advantages, as well as the technical and ecosystem limitations, of remote sensing methods compared with field methods for quantifying soil erosion. We also discuss why we chose to use aerial photogrammetry methods as opposed to available LiDAR or synthetic aperture radar.

Methods

Study Area

The study area for this project was on Shay Mesa (lat 37.9858°N, long 109.5575°W), a 31-ha Upland Shallow loam piñon-juniper site (Site ID: R035XY315UT, USDA Soil Conservation Service, 1991) in southeastern Utah (Fig. 1). Shay Mesa is located approximately 25 km northwest of Monticello, Utah, at an elevation of 2237 m with an average slope of 8 degrees. The mean annual maximum and minimum temperatures are 18.2°C and 3.0°C, respectively (PRISM Climate Group, 2013). The mean annual precipitation is 317 mm and follows a bimodal distribution with monsoonal rains in the summer and snow in the winter. Average annual wind speeds for the study period were 2.8 $m \cdot s^{-1}$ with the prevailing winds from southwest to northeast (USGS CLIM-MET 2014). Shay Mesa is public land managed by the US Department of the Interior's Bureau of Land Management.

Vegetation Treatments

Shay Mesa is dominated by two-needle piñon (*Pinus edulis* Engelm.) and Utah juniper (*Juniperus osteosperma* [Torr.] Little). Other common native plants found within the study site included mountain big sagebrush (*Artemisia tridentata* Nutt. ssp. vaseyana [Rydb.] Beetle), broom snakeweed (*Gutierrezia sarothrae* [Pursh] Britton & Rusby), Indian ricegrass (*Achnatherum hymenoides* [Roem. & Schult.] Barkworth), and blue grama (Bouteloua gracilis [Willd. ex Kunth] Lag. ex Griffiths). In the summer of 2009, a vegetation treatment was conducted to reduce wildfire fuels. Three vegetation removal methods were tested to determine the best method to promote native understory species growth while preventing exotic grass establishment and minimizing soil erosion (see Fig. 1). The methods included mechanical mastication (*M*), lopping of vegetation with the slash collected in piles and then burned (*P*), and lopping of vegetation followed by a broadcast burn

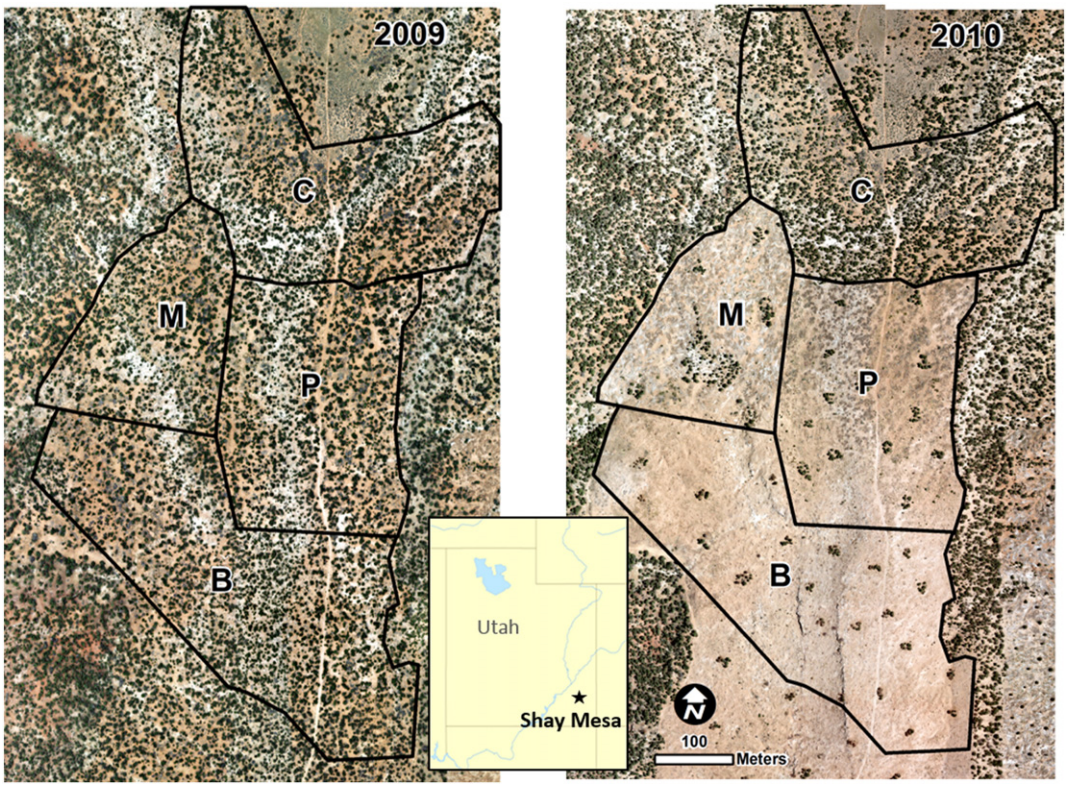

Figure 1. Location of the Shay Mesa study area in southern Utah, United States, showing the treatment configuration and aerial views of the study area before (2009) and after (2010) treatment. The treatments included mechanical mastication *(M);* lopping of vegetation with the slash collected in piles and then burned *(P);* and lopping vegetation with the slash scattered and followed by a broadcast burn *(B)*. An additional area was left untreated to serve as a control site *(C)*.

(*B*). An additional area was left untreated to serve as a control site (*C*). As a substantial amount of soil movement was anticipated with the treatments, this experiment provided an ideal scenario to evaluate DEM differencing for soil erosion measurement over a relatively short time span of a year.

Field Data Collection

To measure sediment flux facilitated primarily by water, small silt fences were installed ($n = 120$, 30 per treatment; Fig. 2) throughout the study area. Silt fences for the *C*, *P*, and *B* treatments were established in July 2009, whereas fences for the *M* treatment were established in October 2009, each immediately after the vegetation treatments. From random points within each treatment, the silt fences were established across the closest and most prominent water flow path less than 1-m wide. Care was taken to ensure that the silt fences were not catching sediment from a neighboring treatment. Silt fences were made of steel mesh (0.54-mm opening size) supported by two rebar rods. Each had a sediment capture surface of 60 cm × 15 cm (0.09 m^2) and a backstop that was 25 cm tall. Sediment (including mineral soil and organic material) that flowed onto the fence surface was collected, dried, and weighed. Over the course of the year, sediment was collected in October, November, and December of 2009 and April, June, and July of 2010.

To measure wind-borne sediment flux, we installed 8 Big Springs Number Eight (BSNE; Fryrear, 1986) wind-aspirated dust samplers (see Fig. 2) in each treatment for a total of 32 across the study area. Dust samplers for the *C*, *P*, and *B* treatments were established in July 2009, while dust samplers for the *M* treatment were established in October 2009. The location of each dust sampler was random within each treatment. The samplers consisted of a single rotating dust collector positioned 15 cm above the soil surface (the closest to the surface it can operate) in order to intercept moving sediment close to the ground where the greatest proportion of transport typically occurs (Fryrear et al., 1991; Ellis et al., 2009). The sampling slot on each dust collector was 0.001 m^2. Dry mineral soil and organic material were collected, dried, and weighed in October, November, and December of 2009 and April, June, and July of 2010.

We conducted a Kruskal-Wallis one way analysis of variance (ANOVA; Chan and Walmsley, 1997) on ranks to test the hypothesis that sediment flux rates were different between treatments as collected by the silt fences and dust samplers. Pairwise comparisons were conducted using a Tukey's test.

We also collected soil samples to measure bulk density ($\frac{solid\ dry\ soil\ mass}{soil\ volume}$), which was used to estimate mass of soil movement ($t \cdot ha^{-1} \cdot y^{-1}$) from the volumetric estimates of DEM differencing (m^3). In 2009 before the vegetation treatments, we collected 40 soil samples from random locations in each treatment. In 2010 after the vegetation treatments, those same locations were resampled 1 m away from the original sample. Soil was collected with polyvinyl chloride coring cylinders (diameter = 5.3 cm, height = 5 cm, volume = 110.31 cm^3) and oven-dried. With spatially explicit samples, bulk density can be estimated across unsampled areas with interpolation methods such as used by Schneider et al. (2011). However, the locational accuracy of our bulk density measures were poor relative to the imagery (1–10 m), so interpolating would assign incorrect bulk density values to individual pixels. Instead, we divided each of the treatment areas into two approximately similar-sized areas (i.e., 8 subtreatments total) and estimated the mean bulk density (sensu Martínez-Casasnovas, 2003; Thoma et al., 2005; Nichols, 2006) for each subtreatment using data from both years.

Because averaging a heterogeneous soil trait like bulk density may introduce some uncertainty in estimating soil mass, the soil movement we report includes the range of soil mass calculated from 95% confidence interval of mean bulk density (similar to DeRose et al., 1998). Confidence

Figure 2. Forty overlapping aerial photographs were acquired for the study area in June 2009 and 2010. Field measurements of sediment flux were made using Big Spring Number Eight wind-aspirated dust samplers ($n = 32$) and small silt fences ($n = 120$) within the three treatment areas and control area. The map also shows treatment and control areas divided into subtreatments, which were used to estimate average bulk density and local precision error thresholds.

intervals were calculated separately for erosion and deposition in each subtreatment. We calculated the net change (sum of erosion and deposition) confidence interval in each subtreatment following Daniel (1999):

$$\overline{x}_1 + \overline{x}_2 \pm t\sqrt{\frac{s_1^2}{n_1} + \frac{s_2^2}{n_2}} \quad (1)$$

where σ_1 and σ_2 are sample means for erosion and deposition, t is the t value for a two-tailed test with $\alpha = 0.05$, s is the standard deviation, and n is the sample size.

Image Acquisition

High-resolution aerial imagery was taken in June 23, 2009 (before vegetation treatments) and June 23, 2010 (1 year after treatment) from a Cessna airplane by Aerographics Inc. (Salt Lake City, UT). The images were taken using an UltraCamX (Vexcel Imaging; Graz, Austria) digital frame camera at an average flying height of 480 m above ground level, yielding a ground sampling distance (GSD) of ~4 cm. Images included four bands (blue, green, red, near-infrared) and were recorded at 16-bit depth. A total of 40 images were acquired each year in four flying passes with 60% overlap and 30% sidelap (see Fig. 2). Each image had a ground footprint approximately 300 m along track and 450 m cross track. The 2009 and 2010 image acquisition plans were identical, but the actual coordinates of the camera at time of exposure varied up to 20 m. Precise camera coordinates and aerial orientation were measured using an Applanix POS AV (Leek Crescent Richmond Hill, Ontario, Canada) global navigation satellite system (GNSS) and inertial measurement unit (IMU). The stated absolute positional accuracy of the GNSS is 0.05−0.30 m, roll and pitch accuracy is 0.005°, and true heading accuracy is 0.008°.

A consequence of acquiring the imagery before the treatments was that the disturbance caused by implementing the treatments was included in the DEM change detection and could not be uncoupled from erosion/deposition. This proved to be problematic in the *M* treatment where the vegetation was mulched and spread over the treatment area in addition to soil compaction from the heavy machinery. As a result, we excluded the *M* treatment from DEM difference analysis.

Surface Reconstruction

Viewing a single point on the ground from multiple aerial perspectives (i.e., overlapping images) allows for estimation of the height of ground features. Aerial triangulation is the basis for quantitatively deriving these heights by establishing a geometric relationship among the image, camera, and ground from multiple aerial perspectives (Wolf and Dewitt, 2000). Using ERDAS LPS 2013 (Intergraph; Huntsville, AL), we performed self-calibrating least square bundle block triangulation (McGlone, 2013) followed by digital image matching to create three-dimensional (3D) point clouds of the study area surface in 2009 and 2010 (Fig. 3A). To improve DEM coregistration, we used a multitemporal bundle block approach (Korpela, 2006; Mondino and Chiabrando, 2008), meaning the 2009 ($n = 40$) and 2010 ($n = 40$) images were processed in the same bundle solution. This technique has not been widely applied in other photogrammetric studies of soil erosion but is promising for topographic change studies because it puts both point clouds into the same coordinate system to reduce coregistration errors (Mondino and Chiabrando, 2008). For comparison, we created DEMs for 2009 and 2010 using separate bundle blocks.

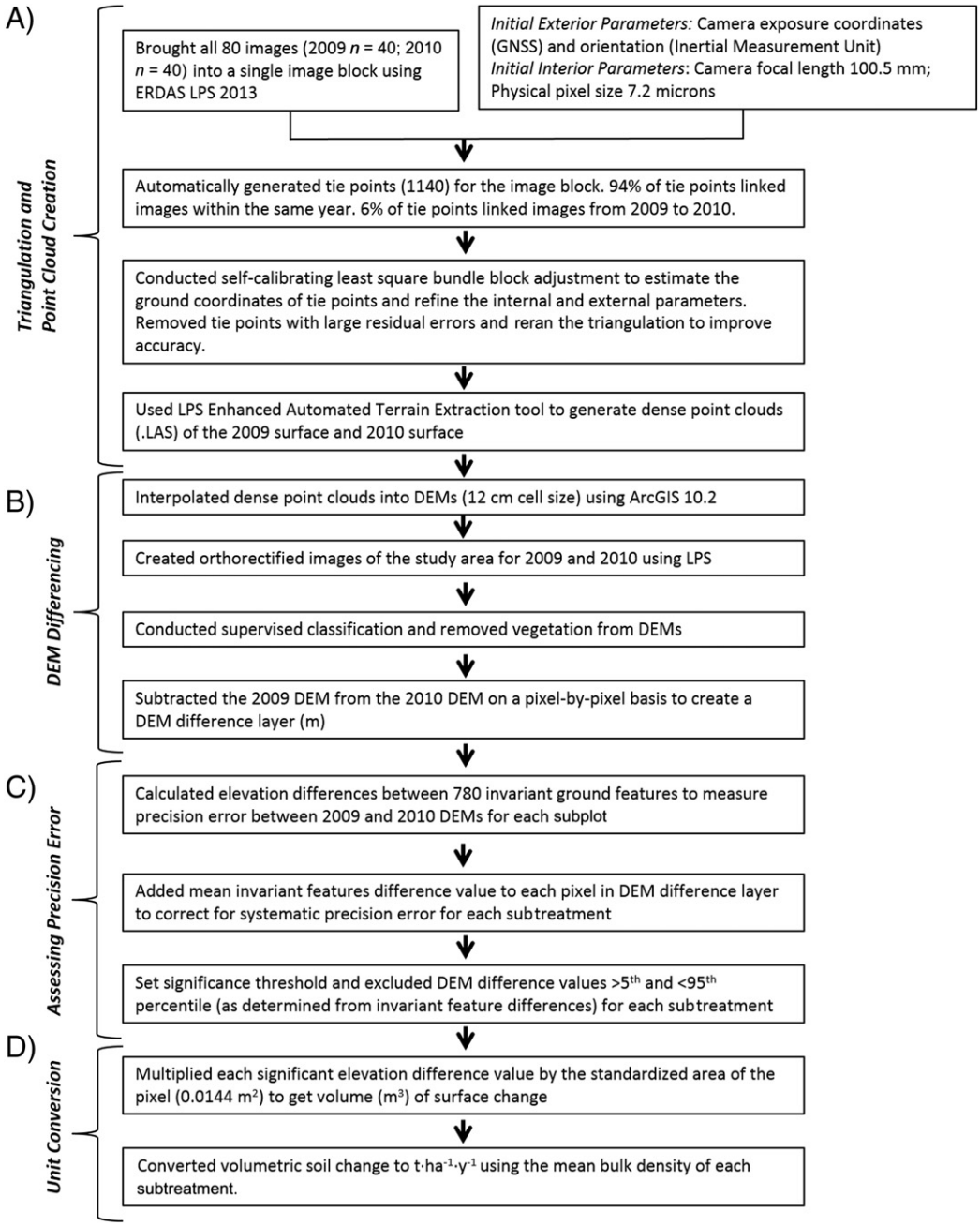

Figure 3. The image processing workflow began with **A,** photogrammetric methods to create three-dimensional surface point clouds from overlapping aerial images. **B,** The point clouds are brought into a geographic information system where they are transformed into digital elevation models (DEMs) and subtracted from one another to create a DEM difference layer showing elevation change between 2009 and 2010. **C,** Model precision is assessed with invariant ground features, and insignificant elevation differences are removed from the model. **D,** Finally, the significant elevation differences are converted to a conventional mass unit of $t \cdot ha^{-1} \cdot y^{-1}$.

Known as direct georeferencing, the use of high-precision GNSS/IMU systems used to record camera location and attitude during image acquisition has made it possible to forego ground control in the triangulation process (Mostafa and Hutton, 2001). As we were primarily interested in achieving data collection efficiencies, we did not collect ground control and instead used estimates of exposure station coordinates (X, Y, Z) and attitude (roll, pitch, heading) from the onboard GNSS/IMU as initial estimates of exterior orientation. The point clouds we created were in a Universal Transverse Mercator projected coordinate system. One potential drawback of direct georeferencing is that the random error contained within the GNSS/IMU data could be larger than the error in surveyed ground control, leading to less accurate ground coordinates in the imagery (Cramer, 2001; Mostafa et al., 2001; Skaloud, 2007).

Success in estimating the X, Y, and Z coordinates of a ground feature depends on the ability to identify the same ground feature in two or more overlapping images (i.e., image matching). We specified the image-matching algorithm to find and create a point every other pixel (8-cm spacing), which was nearly 48 million possible points for the study area. For the 2009 imagery, 57% of the points were correctly matched and for the 2010 imagery, 67% of the points were matched. Point matching was more successful on bare ground (72% for 2009, 71% for 2010) compared with shrubs and trees (37% for 2009, 46% for 2010). Using ArcGIS 10.2 (ESRI, Redlands, CA), we used natural neighbor interpolation on the point clouds to create DEMs for 2009 and 2010 (Fig. 3B). The final GSD of the DEMs was chosen to be 12 cm to reduce raster processing time while being fine enough to distinguish between vegetation and bare ground areas. We also created 4-cm GSD orthorectified images for 2009 and 2010 to classify the study area as vegetation or nonvegetation.

With photogrammetry, it is not possible to estimate soil surface elevations (and thereby soil movement) beneath tree and shrub canopies if the ground features are not visible. Instead of attempting to interpolate below-canopy erosion from nearby visible pixels (see Gillan et al., 2014), we excluded from the analysis all areas that were covered by vegetation canopies in 2009 (48% of study area). We identified vegetation in the orthorectified images using a maximum likelihood supervised classification (Jensen, 2005) of the four image bands combined with a slope threshold (calculated from the pretreatment DEM) corresponding to the elevation change between the ground surface and the canopy of trees and shrubs. A slope threshold of 58 degrees maximized our ability to discriminate vegetation from nonvegetation and was an improvement from only using image spectra (Fig. 3B). We assessed 200 random points on the study area imagery to validate the classification (90% overall accuracy). Once vegetation areas were removed, we subtracted the 2009 DEM from the 2010 DEM on a pixel-by-pixel basis to create a DEM difference product.

Assessing Digital Elevation Model Precision

For this change detection study we were primarily interested in the precision or repeatability of the DEMs. To measure true soil elevation change, it was necessary to identify model precision error due to triangulation and DEM construction (Wheaton et al., 2010; Milan et al., 2011). Moffitt and Mikhail (1980) provide a theoretical framework for estimating the X, Y, Z precision of a surface point. In ideal cases (i.e., when the aerial triangulation inputs are error-free, planimetric (σ_X, σ_Y and height (σ_Z) precision of ground coordinates can be estimated using:

$$\sigma_X = \sigma_Y = \sigma_p \cdot S \tag{2}$$

$$\sigma_Z = \sigma_p \cdot S \cdot \frac{H}{B} \tag{3}$$

where H is the flying height, B is the distance between the centers of two successive images, S is the image scale, and σ_p is the parallax accuracy estimated as $\sqrt{2}\sigma_i$, where σ_i is the standard error of the image coordinate measurements in two images, generated while choosing tie points. The standard error of the image coordinates measurements is a function of the image resolution and the level at which point features can be detected in the images. For most automatic tie point detection algorithms, σ_i is typically one-third of the camera physical pixel size. For this study the flight height *(H)* was 480 m above ground level, the distance between the centers of two successive images *(B)* was approximately 120 m, the image scale *(S)* was 4 444 (i.e., 1:4 444), and σ_i was 2.4 μm, which is one-third of the physical pixel size for UltraCamX (7.2 μm). From these equations our expected precision was:

$$\sigma_X = \sigma_Y = 0.015 \text{ m}$$
$$\sigma_Z = 0.06 \text{ m}$$

Because image orientation parameters are not error free, a practical way to quantify vertical precision error in the DEMs was necessary. From the images, we identified 780 invariant ground features that were assumed to remain the same elevation between successive years (Figs. 3C, 4). These included large rocks and logs that did not appear to move between 2009 and 2010. The elevation difference of these features between years provided a spatially explicit view of vertical error between the models (DeRose et al., 1998; Martínez-Casasnovas et al., 2003; Gessesse et al., 2010), enabling us to assign uncertainty to each pixel in the DEM difference product. Vertical error of the invariant feature differences varied between the eight subtreatment areas (Kruskal-Wallis one-way analysis of variance [ANOVA] on ranks, $H = 85.792$, $p = < 0.001$). Accordingly, we used the mean invariant feature differences for each subtreatment to correct for systematic errors between the models by adding the invariant feature difference mean to every cell in the DEM difference product (see DeRose et al., 1998).

Because invariant feature difference values are positively spatially autocorrelated (Moran's $I = 0.21$, $p = < 0.0001$), parametric significance tests may produce inflated Type I error rates (Dale and Fortin, 2002). The invariant feature differences also failed normality tests (Shapiro-Wilk, $W = 0.954$, $p = < 0.001$). Accordingly, we used a nonparametric approach to determine areas of significant soil surface change within each subtreatment using a theshold level of detection at the 5th and 95th percentiles. Only DEM difference values in the upper or lower fifth percentile were considered to be significant changes in soil surface (Fig. 3C). This nonparametric approach limited the potential for Type I errors (i.e., reporting soil movement when it did not actually occur).

Each pixel in the DEM difference image represented the change in elevation in meters between years. We calculated volume (m^3) of soil movement by multiplying each pixel by the standardized area of the pixel (0.0144 m^2; Fig. 3D). We then estimated the mass ($t \cdot ha^{-1} \cdot y^{-1}$) of soil movement on the basis of bulk density of the soil samples from each treatment. This enabled us to estimate soil mass decrease (erosion), increase (deposition), and net change for the whole study area and for each treatment. We also calculated the total surface area of each treatment that experienced significant elevation change.

Comparison of Digital Elevation Model Difference and Field Measurements

While measurements from the field methods are indicators of sediment transport, DEM differencing measures topographic change from which the effects of sediment transport processes over time can be inferred. Accordingly, the field measurements are not directly comparable with DEM differencing, but general agreement in magnitude and pattern of results from both the field and DEM differencing should be expected. We visually assessed the agreement between the field and imagery methods and conducted Pearson product moment correlations between sediment flux estimates and DEM difference values in each subtreatment. We also compared the erosion rank order of treatments (i.e., which treatments had the most and least erosion) between the field and DEM difference methods.

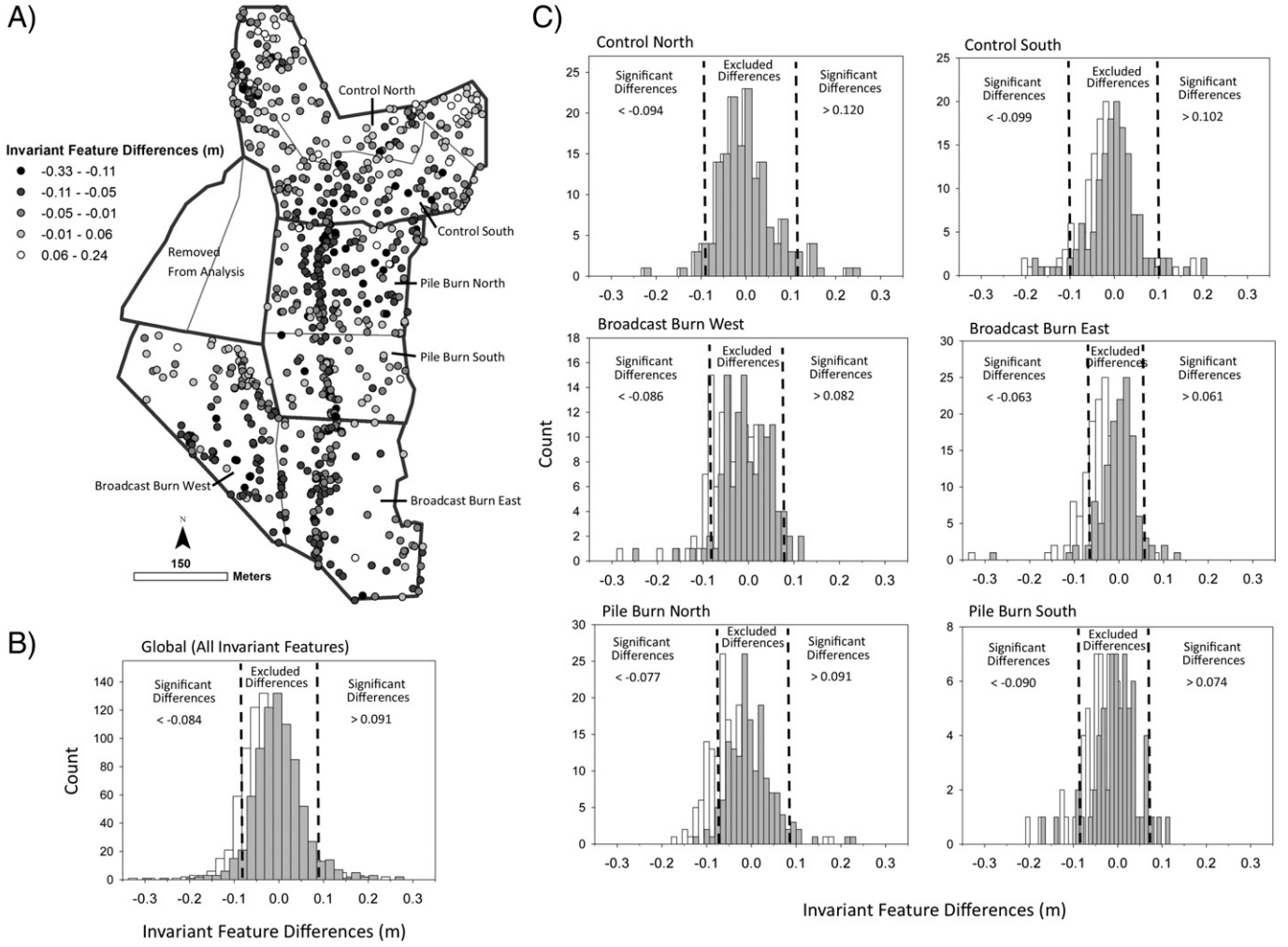

Figure 4. A, The geographic distribution of invariant features (rocks, logs) chosen to assess precision error between 2009 and 2010 digital elevation models (DEMs; 2009 elevations subtracted from 2010 elevations). **B,** The histogram of all invariant features differences. White bars represent the original histogram while gray bars represent the histogram shifted (using invariant feature difference mean) to eliminate systematic errors between DEMs. **C,** The invariant feature difference histograms for each subtreatment. A percentile threshold was used to separate precision error from actual surface change. For each subtreatment, DEM differences >5 percentile and < 95 percentile (as determined from the invariant feature differences) were excluded from the analysis.

Results

Digital Elevation Model Precision

Analysis of all the invariant feature differences showed that photogrammetric processing using the multitemporal bundle block approach had better DEM coregistration compared with the separate bundle approach (Table 1). Although there was a larger vertical systematic shift between the DEMs using the multitemporal bundle method, the standard deviation of the invariant feature differences was roughly half using the multitemporal bundle method (0.057 m compared with 0.10 m), which generated a smaller error range and enhanced our ability to detect true surface change. The remaining results in this paper use the multitemporal bundle approach only.

Each subtreatment had unique error estimates that provided an increased level of detail compared with the global error estimate, which approximated an average across the study area (see Table 1; Fig. 4). On average, the 2010 DEM was systematically lower in elevation

Table 1
Local digital elevation model (DEM) precision error as measured from invariant feature elevation differences in 2009 and 2010 imagery. Photogrammetric processing was carried out using a multitemporal bundle block to reduce precision error between DEMs. For comparison, processing using separate bundles is also presented.

Treatment	Invariant features *n*	Invariant feature mean elevation difference (m)	Standard deviation (m)	Significant change threshold 5th percentile	95th % percentile	Precision error range
All Treatments (separate bundles)	*780*	−0.01	0.10	−0.15	0.11	*0.260*
All Treatments	*780*	−0.031	0.057	−0.084	0.091	0.175
Control North	159	−0.006	0.082	−0.094	0.120	0.214
Control South	144	−0.024	0.059	−0.099	0.102	0.201
Broadcast West	121	−0.035	0.053	−0.086	0.082	0.168
Broadcast East	129	−0.048	0.044	−0.063	0.061	0.124
Pile Burn North	163	−0.049	0.051	−0.077	0.091	0.168
Pile Burn South	65	−0.035	0.049	−0.090	0.074	0.164

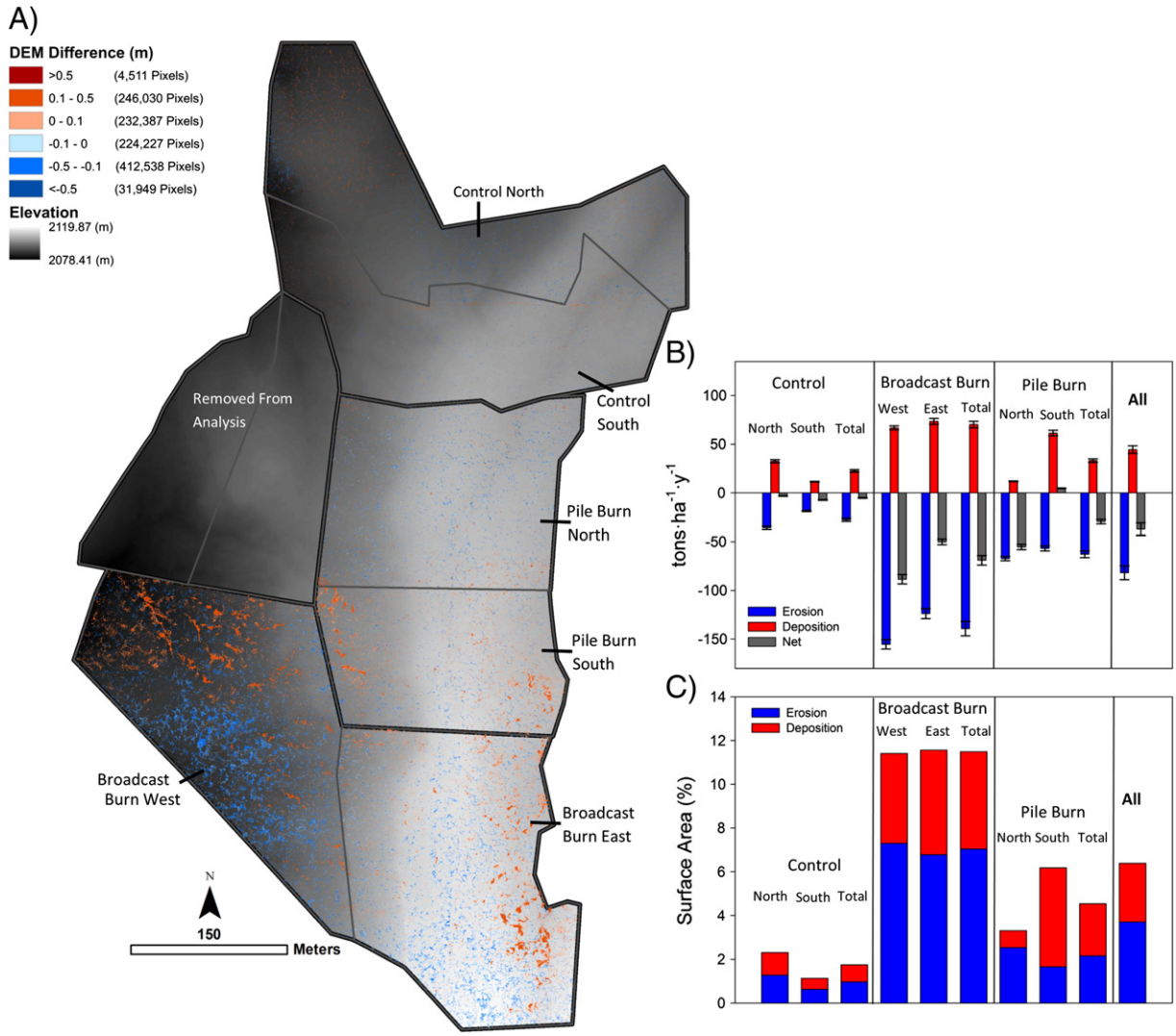

Figure 5. A, Significant vertical differences between 2009 and 2010 digital elevation models (DEMs). Blue colors represent soil erosion while orange and red colors indicate soil deposition. **B,** Erosion, deposition, and net soil mass change from 2009 to 2010 for each treatment area. Included with each bar is a 95% confidence interval for uncertainty in bulk density estimates. **C,** Surface area (%) of each treatment exhibiting significant change.

compared with the 2009 DEM (mean = −0.031 m). This same bias occurred in each of the subtreatments to varying degrees. Adding the invariant feature mean to each cell in the DEM difference product shifted the histogram means near zero, thus eliminating most of the systematic error. The variability of the invariant feature differences as measured by the significant change threshold was also unique in each subtreatment. The *C* north subtreatment had the largest error range with a significant change threshold < −0.094 m and > 0.120 m, while the smallest error range occurred in the *B* east subtreatment (< −0.063 m and > 0.061 m). The global significance threshold approximated an average between the subtreatments (< −0.084 m and > 0.091 m).

Digital Elevation Model Difference

The DEM difference model, depicting significant surface elevation changes from 2009 to 2010 due to soil erosion and deposition across the study area, showed more soil movement in the southern subtreatments of the study area (*B* west, *B* east, *P* south) compared with the northern subtreatments (*C* north, *C* south, *P* north; Fig. 5). Though it cannot be seen in the figure, most of the deep soil deposits appear to be in what were previously water flow paths.

The confidence intervals used to account for uncertainty in bulk density produced relatively narrow error ranges when calculating soil movement mass (between ± 0.21 and ± 7.44 $t \cdot ha^{-1} \cdot y^{-1}$; Table 2; Fig. 5B). The uncertainty in soil mass did not seem to affect the comparison between treatments or subtreatments. Comparing soil movement rates between the treatments revealed that the *B* treatment experienced the most erosion (−139.22 ± 7.44 $t \cdot ha^{-1} \cdot y^{-1}$) and deposition (70.31 ± 3.38 $t \cdot ha^{-1} \cdot y^{-1}$) followed by the *P* treatment and lastly *C* (Table 3). Rank order for erosion in the subtreatments followed the same general order as the treatments. For subtreatment deposition, the same rank order persisted except that the *C* north subtreatment had more deposition than the *P* north subtreatment. Over the whole study area there was a net soil loss (−37.24 $t \cdot ha^{-1} \cdot y^{-1}$) suggesting soil was transported off of the study area by wind or water. All of the subtreatments exhibited net soil loss except for the *P* south subtreatment.

The DEM differencing approach to assessing erosion also allows for analysis of areas affected by deposition and/or erosion. Of the whole study area, 6.39% exhibited significant soil movement (3.71% erosion, 2.68% deposition; see Table 2; Fig. 5C). Every subtreatment except *P* south exhibited more surface area of erosion than surface area of deposition. The *B* treatment had the most erosion (7.04%) and deposition (4.45%) surface area, followed by treatment *P* and *C* (see Table 3). The rank of subtreatment erosion surface area followed the same general

Table 2
Soil volume and mass change between 2009 and 2010 digital elevation models (DEMs) and total surface area experiencing significant change using local precision error thresholds (<5th percentile and >95th percentile).

Treatment	*DEM difference local error threshold* ($m^3 \cdot y^{-1}$)	*DEM difference local error threshold* ($m^3 \cdot ha^{-1} \cdot y^{-1}$)	CI_{95} *mean bulk density*	*DEM difference local error threshold* ($tons \cdot y^{-1}$)	*DEM difference local error threshold* ($tons \cdot ha^{-1} \cdot y^{-1}$)	*Significant change (surface area %)*
Control North (4.47 ha)	Erosion: −131.50	Erosion: −29.41	1.22 ± 0.06	Erosion: −160.43 ± 7.89	Erosion: −35.88 ± 1.76	Erosion: 1.28%
	Deposition: 119.28	Deposition: 26.68	1.22 ± 0.06	Deposition: 145.52 ± 7.15	Deposition: 32.54 ± 1.59	Deposition: 1.03%
	Net: −12.22	**Net: −2.72**	1.22 ± 0.08	**Net: −14.91 ± 0.97**	**Net: −3.31 ± 0.21**	**Total: 2.31%**
Control South (4.0 ha)	Erosion: −59.69	Erosion: −14.92	1.25 ± 0.04	Erosion: −74.61 ± 2.39	Erosion: −18.65 ± 0.59	Erosion: 0.63%
	Deposition: 36.32	Deposition: 9.08	1.25 ± 0.04	Deposition: 45.40 ± 1.45	Deposition: 11.35 ± 0.36	Deposition: 0.50%
	Net: −23.36	**Net: −5.84**	1.25 ± 0.07	**Net: −29.21 ± 1.62**	**Net: −7.3 ± 0.40**	**Total: 1.13%**
Control (8.47 ha)	Erosion: −191.19	Erosion: −22.57	1.23* ± 0.07	Erosion: −235.04 ± 13.38	Erosion: −27.74 ± 1.57	Erosion: 0.97%
	Deposition: 155.6	Deposition: 18.37	1.23* ± 0.07	Deposition: 190.92 ± 11.20	Deposition: 22.54 ± 1.32	Deposition: 0.78%
	Net: −35.59	**Net: −4.20**	1.23* ± 0.10	**Net: −44.12 ± 3.55**	**Net: −5.20 ± 0.41**	**Total: 1.75%**
Broadcast Burn West (5.06 ha)	Erosion: −609.28	Erosion: −120.41	1.29 ± 0.04	Erosion: −785.97 ± 24.37	Erosion: −155.32 ± 4.81	Erosion: 7.3%
	Deposition: 262.41	Deposition: 51.85	1.29 ± 0.04	Deposition: 338.50 ± 10.50	Deposition: 66.88 ± 2.07	Deposition: 4.11%
	Net: −346.86	**Net: −68.56**	1.29 ± 0.07	**Net: −447.47 ± 24.25**	**Net: −88.44 ± 4.79**	**Total: 11.41%**
Broadcast Burn East (5.25 ha)	Erosion: −536.74	Erosion: −102.23	1.21 ± 0.05	Erosion: −649.45 ± 26.84	Erosion: −123.69 ± 5.11	Erosion: 6.78%
	Deposition: 319.34	Deposition: 60.82	1.21 ± 0.05	Deposition: 386.40 ± 15.96	Deposition: 73.59 ± 3.04	Deposition: 4.78%
	Net: −217.39	**Net: −41.41**	1.21 ± 0.07	**Net: −263.05 ± 15.20**	**Net: −50.10 ± 2.89**	**Total: 11.56%**
Broadcast Burn (10.31 ha)	Erosion: −1146.02	Erosion: −111.15	1.25* ± 0.06	Erosion: −1435.42 ± 76.75	Erosion: −139.22 ± 7.44	Erosion: 7.04%
	Deposition: 581.75	Deposition: 56.42	1.24* ± 0.06	Deposition: 724.9 ± 34.86	Deposition: 70.31 ± 3.38	Deposition: 4.45%
	Net: −564.27	**Net: −54.73**	1.25* ± 0.09	**Net: −710.52 ± 50.73**	**Net: −68.91 ± 4.92**	**Total: 11.49%**
Pile Burn North (4.05 ha)	Erosion: −219.53	Erosion: −54.20	1.24 ± 0.04	Erosion: −272.21 ± 8.78	Erosion: −67.20 ± 2.16	Erosion: 2.54%
	Deposition: 38.91	Deposition: 9.60	1.24 ± 0.04	Deposition: 48.24 ± 1.56	Deposition: 11.90 ± 0.38	Deposition: 0.77%
	Net: −180.62	**Net: −44.59**	1.24 ± 0.06	**Net: −223.97 ± 10.83**	**Net: −55.29 ± 2.67**	**Total: 3.31%**
Pile Burn South (3.04 ha)	Erosion: −133.75	Erosion: −43.99	1.29 ± 0.06	Erosion: −172.53 ± 8.03	Erosion: −56.74 ± 2.64	Erosion: 1.66%
	Deposition: 144.88	Deposition: 47.65	1.29 ± 0.06	Deposition: 186.89 ± 8.69	Deposition: 61.46 ± 2.85	Deposition: 4.52%
	Net: 11.12	**Net: 3.66**	1.29 ± 0.08	**Net: 14.36 ± 0.87**	**Net: 4.72 ± 0.28**	**Total: 6.18%**
Pile Burn (7.09 ha)	Erosion: −353.28	Erosion: −49.82	1.25* ± 0.07	Erosion: −444.74 ± 24.69	Erosion: −62.72 ± 3.48	Erosion: 2.16%
	Deposition: 183.79	Deposition: 25.92	1.27* ± 0.07	Deposition: 235.13 ± 12.85	Deposition: 33.16 ± 1.81	Deposition: 2.38%
	Net: −169.49	**Net: −23.90**	1.23* ± 0.10	**Net: −209.61 ± 16.94**	**Net: −29.56 ± 2.38**	**Total: 4.54%**
All Treatments (25.89 ha)	Erosion: −1690.49	Erosion: −65.29	1.25* ± 0.11	Erosion: −2115.20 ± 185.89	Erosion: −81.69 ± 7.17	Erosion: 3.71%
	Deposition: 921.14	Deposition: 35.57	1.24* ± 0.11	Deposition: 1150.95 ± 101.24	Deposition: 44.45 ± 3.91	Deposition: 2.68%
	Net: −769.35	**Net: −29.71**	1.25* ± 0.16	**Net: −964.25 ± 123.07**	**Net: −37.24 ± 4.75**	**Total: 6.39%**

* Values were derived, not collected in the field.

order as the treatments. The rank order of subtreatment deposition surface area from most to least was *B* east, *P* south, *B* west, *C* north, *P* north, and *C* south.

Comparison of Digital Elevation Model Difference and Field Measurements

Sediment flux rates were shown to be significantly different by treatment for dust samplers ($H = 25.324$, $P < 0.001$) and silt fences ($H = 77.237$, $P < 0.001$). For both field methods, the Tukey pairwise test found significant differences between *B* versus *C* and *P* versus *C* treatments ($P < 0.01$) but did not find significant differences between *B* versus *P* treatments. Between 2009 and 2010, more sediment was collected by the dust samplers (31.417 $kg \cdot m^{-2} \cdot d^{-1}$) than by the silt fences (18.022 $kg \cdot m^{-2} \cdot d^{-1}$) despite the fact that there were many more silt fences ($n = 120$) than dust samplers ($n = 32$; Table 4).

Field measured sediment flux exhibited a similar spatial pattern of soil movement compared with DEM differencing (Fig. 6). Areas of erosion and deposition were often complemented with higher levels of sediment capture by the dust samplers and silt fences, and areas without significant soil movement often had lower sediment capture. Pearson correlation between DEM differencing and field measurements indicated strong positive linear relationships between captured sediment and topographic change (Table 5). By treatment, sediment captured by silt fences and dust samplers had the same rank order as the DEM difference measurements of erosion and deposition (see Fig. 6B; Table 3). Treatment *B* had the highest flux rates, followed by treatment *P* and, finally, *C*.

Discussion

Our results demonstrate the ability of photogrammetric DEM differencing to broadly characterize geographic patterns of soil surface change on rangeland landscapes. Along with assessing relative erosion rates between treatments, photogrammetric DEM differencing enabled assessment of the spatial patterns in net losses and gains and identification of the proportion of the landscape experiencing significant change.

Sediment-flux field methods and DEM differencing provided complementary information and thus a more complete picture of soil movement than any single method could alone. DEM differencing gave an estimate of the net result of processes that cause soil erosion and detailed spatial data on how erosion and deposition are manifest on the landscape but did not directly discriminate between those processes (i.e., wind and water). In contrast, the field methods provided estimates of fluxes attributable to differing processes but did not provide information on specific areas of soil loss and gain.

Sediment is being carried by wind or water between the treatments, which could confound the ability to detect treatment differences from field data alone. From the field samplers we can see the relative amount of sediment flux in each treatment but need the DEM difference to help infer where the sediment is coming from, where it is going, and knowing the magnitude of exchange between the treatments. For example, the DEM difference informed us that the *P* south subtreatment was the only subtreatment to exhibit more deposition than erosion. Knowing that the dominant wind direction is from southwest to northeast, it is likely that sediment from the adjacent *B* treatment is being transported into the dust samplers of *P* south.

Our ability to identify significant vertical soil change of ±8–9 cm and greater was sufficient for the large amount of soil movement exhibited on the study area and could be used to monitor erosion in other scenarios where erosion potential is very high (e.g., postfire). Compared with the two other known studies employing photogrammetric DEM differencing at a comparable scale, our error range was quite similar to one study (Martínez-Casasnovas et al., 2003 reported ± 0.088 m) and more precise than the other (Lane et al., 2003 reported ± 0.32 m). Both studies used surveyed ground control points. Had we used ground control, the vertical precision would have been closer to the theoretical estimate of ± 6 cm

Table 3
Rank order (most to least).

Metric	Treatments	Subtreatments
DEM Erosion Mass $\mathbf{tons \cdot ha^{-1} \cdot y^{-1}}$	1. Broadcast Burn 2. Pile Burn 3. Control	1. Broadcast West 2. Broadcast East 3. Pile North 4. Pile South 5. Control North 6. Control South
DEM Deposition Mass $\mathbf{tons \cdot ha^{-1} \cdot y^{-1}}$	1. Broadcast Burn 2. Pile Burn 3. Control	1. Broadcast East 2. Broadcast West 3. Pile South 4. Control North 5. Pile North 6. Control South
DEM Surface Area Erosion **%**	1. Broadcast Burn 2. Pile Burn 3. Control	1. Broadcast West 2. Broadcast East 3. Pile North 4. Pile South 5. Control North 6. Control South
DEM Surface Area Deposition **%**	1. Broadcast Burn 2. Pile Burn 3. Control	1. Broadcast East 2. Pile South 3. Broadcast West 4. Control North 5. Pile North 6. Control South
Dust Samplers $\mathbf{g \cdot m^{-2} \cdot d^{-1}}$	1. Broadcast Burn 2. Pile Burn 3. Control	1. Broadcast East 2. Broadcast West 3. Pile South 4. Pile North 5. Control South 6. Control North
Silt Fences $\mathbf{g \cdot m^{-2} \cdot d^{-1}}$	1. Broadcast Burn 2. Pile Burn 3. Control	1. Broadcast East 2. Broadcast West 3. Pile South 4. Pile North 5. Control South 6. Control North

(Moffitt and Mikhail, 1980), but with an additional cost of surveying. Detecting more subtle soil erosion (i.e., smaller than ± 6 cm) on rangeland landscapes could be achieved using the same methodology presented in this paper but with higher-resolution imagery, which allows for finer vertical precision. Lower-flying aircraft such as unmanned aerial vehicles would be ideal platforms.

Though erosion rates can vary dramatically on the basis of slope, climate, soil type, and land use, (García-Ruiz et al., 2015) comparing the erosion rates of this study with other studies is useful to generally verify the observed results. Robichaud et al. (2013) reported overland flow sediment yields of 22.2 $mg \cdot ha^{-1} \cdot y^{-1}$ and 38.6 $Mg \cdot ha^{-1} \cdot y^{-1}$ 1 and 2 years after a wildfire, respectively, in a ponderosa pine *(Pinus ponderosa)*—dominated forest in Colorado. In semiarid New South Wales, Australia, Fanning (1994) reported an erosion rate of 86 $t \cdot ha^{-1} \cdot y^{-1}$ using the erosion pin method. In the shrub-dominated desert of southeastern Arizona, Nearing et al. (2005), using the cesium^{137} method, reported a net soil loss of 4.3 $t \cdot ha^{-1} \cdot y^{-1}$. In a study conducted in a piñon-juniper woodland in northern New Mexico (similar to Shay Mesa) Wilcox et al. (1996) reported an erosion rate of 47 $t \cdot ha^{-1} \cdot y^{-1}$ using the erosion bridge method. The erosion rates in these studies indicate that a net soil loss of 37.24 ± 4.75 $t \cdot ha^{-1} \cdot y^{-1}$ on Shay Mesa is a plausible figure.

With photogrammetry, our ability to quantify soil surface change is obscured by vegetation canopy, which may limit the utility of the technique in some environments. For example, we can get a more complete picture of erosion in shrublands with high proportions of bare ground compared with grasslands or other systems with more vegetation cover. Our decision to mask out areas of vegetation meant that soil moving in or out of the masked areas is unaccounted for, and thus the true mass and surface changes could be different than what we estimated. Surface obscuration caused by masticated vegetation was the primary reason we removed the *M* treatment from the analysis.

Terrestrial and airborne LiDAR systems are increasingly being used to generate DEM differencing products over large areas as an alternative to aerial photogrammetry (Perroy et al., 2010). A distinct advantage of LiDAR is its ability to estimate surface elevations below vegetation canopies, which may give a more complete view of landscape-level erosion in high-canopy situations. Though LiDAR DEM accuracy under vegetation canopy is generally poorer compared with noncanopy areas (Reutebuch et al., 2003; James et al., 2007), this is an improvement compared with photogrammetric methods that cannot see below canopies. Despite the advantage of LiDAR, the strongest case for continuing to use photogrammetry instead is its ability to easily capture spectral data in addition to terrain elevations with one system. Having a coupled LiDAR and camera system increases costs and payload size/weight. This could limit its use with small unmanned aerial vehicles, which are becoming increasingly popular for natural resource science (Rango et al., 2009; Eisenbeiss and Sauerbier, 2011; Anderson and Gaston, 2013). There is also the added challenge of coregistering two-dimensional (2D) optical imagery with 3D LiDAR data (Yang and Chen, 2015). Many resource-monitoring programs are already using aerial photography (Nusser and Goebel, 1997), and with some minor modifications (e.g., digital image acquisition, higher-resolution imagery, adequate image overlap) DEM differencing from photogrammetric techniques could become a standard monitoring procedure with limited additional cost. The progress of softcopy photogrammetry tools such as structure-from-motion have made generating 3D data from 2D images cheaper and easier than ever before (Westoby et al., 2012).

In large monitoring programs, predictive process models have gained traction for broad-scale characterization of rangeland soil erosion. Models such as the Rangeland Hydrology Erosion Model (Nearing et al., 2011), Automated Geospatial Watershed Assessment tool (Goodrich et al., 2011), and Wind Erosion Model (Okin, 2008) are being used extensively in the United States to estimate potential soil erosion on the basis of data inputs such as soil texture, vegetation cover, and slope. These predictive models are useful for evaluating management scenarios but do not directly observe soil movement. Future research could explore DEM differencing to supplement the information these models are generating in the form of model validation or a companion data set that quantitatively tracks surface change over time.

Implications

Minimizing the loss of soil resources is crucial to sustaining the productivity and ecosystem services of rangelands worldwide and protecting their ability to resist disturbance. The key to accomplishing this is reliable techniques for measuring and monitoring the extent and severity of soil erosion. The technique of photogrammetric DEM

Table 4
Big Spring Number Eight (BSNE) dust samplers and silt fence sediment capture from July 2009 to July 2010. Values in each cell are the sums of all samplers in that subtreatment.

Treatment	BSNE dust sampler ($g \cdot m^{-2} \cdot d^{-1}$)	Silt fence ($g \cdot m^{-2} \cdot d^{-1}$)
Control North	86.80	24.24
Control South	103.73	82.28
Control Total	190.54	113.01
Broadcast Burn West	11,635.23	6,383.95
Broadcast Burn East	13,309.26	8,921.37
Broadcast Burn Total	24,944.50	15,305.34
Pile Burn North	750.92	733.48
Pile Burn South	5,531.07	1,998.96
Pile Burn Total	6,281.99	2,604.19
All Treatments	31,417.03	18,022.54

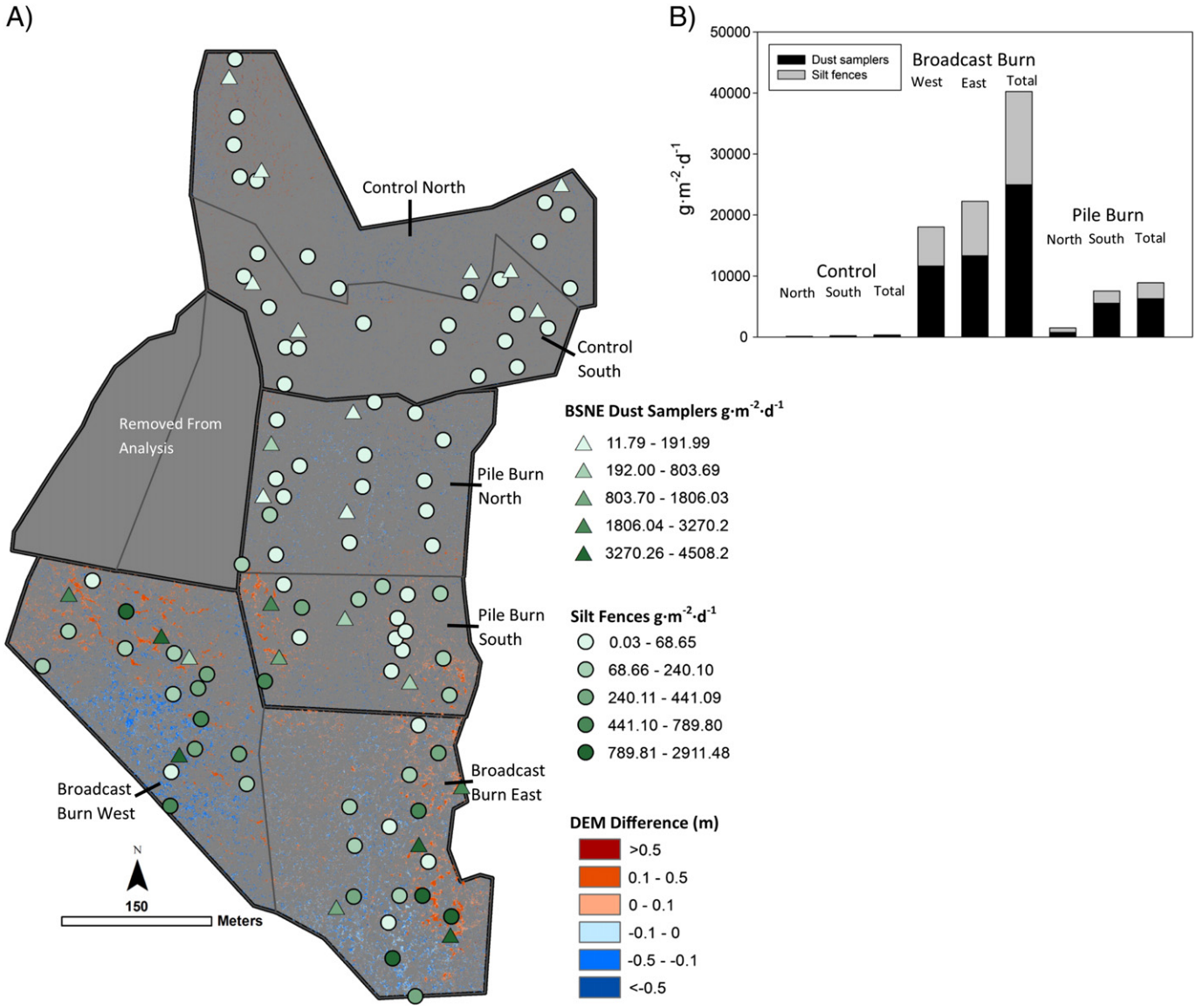

Figure 6. The rate of sediment flux as collected by Big Spring Number Eight dust samplers and silt fences from July 2009 to July 2010. **A,** The field data plotted on the local precision error digital elevation model difference layer. **B,** Sum of captured sediment for each subtreatment.

differencing presented here can provide landscape-scale data on soil loss and redistribution that complements the process-focused field-based techniques that are typically used. Advances in digital photogrammetric techniques and software coupled with an increasing availability of very-high-resolution digital imagery now make it possible to produce estimates of soil surface elevation at a fine enough resolution and with sufficient precision to estimate soil erosion at scales meaningful for management of natural landscapes.

Table 5
Pearson Product Moment Correlations between soil mass change as measured by digital elevation model (DEM) differences ($t \cdot ha^{-1} \cdot y^{-1}$) and soil flux as estimated from sediment traps ($g \cdot m^{-2} \cdot d^{-1}$), grouped by subtreatments.

Comparison	Sample *n*	Coefficient	*P* value
DEM erosion vs. silt fences	6	0.902	0.0140
DEM erosion vs. dust samplers	6	0.904	0.0134
DEM deposition vs. silt fences	6	0.814	0.0485
DEM deposition vs. dust sampler	6	0.907	0.0125

Acknowledgments

For assistance with field sampling, we thank Sarah Castle, Cody Flagg, Heidi Guenther, Conor Morrison, Matt Ross, and Laura Schafenacker. We are grateful to Brian Keating, Gabe Bissonette, and Paul Plemmons from the Bureau of Land Management for treatment implementation.

References

Anderson, K., Gaston, K.J., 2013. Lightweight unmanned aerial vehicles will revolutionize spatial ecology. Frontiers in Ecology and the Environment 11 (3), 138–146. http://dx.doi.org/10.1890/120150.

Betts, H.D., DeRose, R.C., 1999. Digital elevation models as a tool for monitoring and measuring gully erosion. International Journal of Applied Earth Observation and Geoinformation 1 (2), 91–101. http://dx.doi.org/10.1016/s0303-2434(99)85002-8.

Booth, D.T., Cox, S.E., Fifield, C., Phillips, M., Williamson, N., 2005. Image analysis compared with other methods for measuring ground cover. Arid Land Research and Management 19 (2), 91–100. http://dx.doi.org/10.1080/15324980590916486.

Booth, D.T., Cox, S.E., Berryman, R.D., 2006. Point sampling digital imagery with 'Samplepoint'. Environmental Monitoring and Assessment 123 (1), 97–108. http://dx.doi.org/10.1007/s10661-005-9164-7.

Booth, D.T., Cox, S.E., 2008. Image-based monitoring to measure ecological change in rangeland. Frontiers in Ecology and the Environment 6 (4), 185–190. http://dx.doi.org/10.1890/070095.

Brasington, J., Langham, J., Rumsby, B., 2003. Methodological sensitivity of morphometric estimates of coarse fluvial sediment transport. Geomorphology 53 (3–4), 299–316. http://dx.doi.org/10.1016/s0169-555x(02)00320-3.

Bremer, M., Sass, O., 2012. Combining airborne and terrestrial laser scanning for quantifying erosion and deposition by a debris flow event. Geomorphology 138 (1), 49–60. http://dx.doi.org/10.1016/j.geomorph.2011.08.024.

Brown, D.G., Arbogast, A.F., 1999. Digital photogrammetric change analysis as applied to active coastal dunes in Michigan. Photogrammetric Engineering & Remote Sensing 65 (4), 467–474.

Chan, Y., Walmsley, R.P., 1997. Learning and understanding the Kruskal-Wallis one-way analysis-of-variance-by-ranks test for differences among three or more independent groups. Physical Therapy 77, 1755–1761.

Chartier, M.P., Rostagno, C.M., 2006. Soil erosion thresholds and alterative states in north-eastern Patagonian rangelands. Rangeland Ecology & Management 59 (6), 616–624. http://dx.doi.org/10.2111/06-009R.1.

Cramer, M., 2001. Performance of GPS/inertial solutions in photogrammetry. In: Fritsch/Spiller (Ed.), Photogrammetric week 2001. Wichmann Verlag, Heidelberg, Germany, pp. 49–62.

d' Oleire-Oltmanns, S., Marzolff, I., Peter, K.D., Ries, J.B., 2012. Unmanned aerial vehicle (UAV) for monitoring soil erosion in Morocco. Remote Sensing 4, 3390–3416. http://dx.doi.org/10.3390/rs4113390.

Dale, M.R.T., Fortin, M., 2002. Spatial autocorrelation and statistical tests in ecology. Ecoscience 9 (2), 162–167.

Daniel, W.W., 1999. Biostatistics: a foundation for analysis in the health sciences. 7th ed. John Wiley and Sons, New York, NY, USA, p. 152.

DeRose, R.C., Gomez, B., Marden, M., Trustrum, N.A., 1998. Gully erosion in Mangatu Forest, New Zealand, estimated from digital elevation models. Earth Surface Processes and Landforms 23 (11), 1045–1053. http://dx.doi.org/10.1002/(sici)1096-9837(1998110)23:11<1045::aid-esp920>3.0.co;2-t.

Duniway, M.C., Karl, J.W., Schrader, S., Baquera, N., Herrick, J.E., 2011. Rangeland and pasture monitoring: an approach to interpretation of high-resolution imagery focused on observer calibration for repeatability. Environmental Monitoring and Assessment 184 (6), 3789–3804. http://dx.doi.org/10.1007/s10661-011-2224-2.

Eisenbeiss, H., Sauerbier, M., 2011. Investigation of UAV systems and flight modes for photogrammetric applications. The Photogrammetric Record 26 (136), 400–421. http://dx.doi.org/10.1111/j.1477-9730.2011.00657.x.

Ellis, J.T., Li, B., Farrell, E.J., Sherman, D.J., 2009. Protocols for characterizing aeolian mass-flux profiles. Aeolian Research 1 (1–2), 19–26. http://dx.doi.org/10.1016/j.aeolia.2009.02.001.

Fanning, P., 1994. Long-term contemporary erosion rates in an arid rangelands environment in western New South Wales, Australia. Journal of Arid Environments 28 (3), 173–187. http://dx.doi.org/10.1016/s0140-1963(05)80055-2.

Fryrear, D.W., 1986. A field dust sampler. Journal of Soil and Water Conservation 41 (2), 117–120.

Fryrear, D.W., Stout, J.E., Hagen, L.J., Vories, E.D., 1991. Wind erosion: field measurement and analysis. Trans ASAE 34 (1), 155–160. http://dx.doi.org/10.13031/2013.31638.

García-Ruiz, J.M., Beguería, S., Nadal-Romero, E., González-Hidalgo, J.C., Lana-Renault, N., Sanjuán, Y., 2015. A meta-analysis of soil erosion rates across the world. Geomorphology 239, 160–173. http://dx.doi.org/10.1016/j.geomorph.2015.03.008.

Gessesse, G.D., Fuchs, H., Mansberger, R., Klik, A., Rieke-Zapp, D.H., 2010. Assessment of erosion, deposition and rill development on irregular soil surfaces using close range digital photogrammetry. Photogrammetric Record 25, 299–318. http://dx.doi.org/10.1111/j.1477-9730.2010.00588.x.

Gillan, J.K., Karl, J.W., Duniway, M., Elaksher, A., 2014. Modeling vegetation heights from high resolution stereo aerial photography: an application for broad-scale rangeland monitoring. Journal of Environmental Management 144, 226–235. http://dx.doi.org/10.1016/j.jenvman.2014.05.028.

Goodrich, D.C., Guertin, D.P., Burns, I.S., Nearing, M.A., Stone, J.J., Wei, H., Heilman, P., Hernandez, M., Spaeth, K., Pierson, F., Paige, G.B., Miller, S.N., Kepner, W.G., Ruyle, G., McClaran, M.P., Weltz, M., Jolley, L., 2011. AGWA: the automated geospatial watershed assessment tool to inform rangeland management. Rangelands 33 (4), 41–47. http://dx.doi.org/10.2111/1551-501X-33.4.41.

Ecosystems and human well-being: current state and trends. In: Hassan, R.M., Scholes, R., Ash, N. (Eds.), Island Press, Washington DC, USA.

Heng, B.C.P., Chandler, J.H., Armstrong, A., 2010. Applying close range digital photogrammetry in soil erosion studies. Photogrammetric Record 25, 240–265. http://dx.doi.org/10.1111/j.1477-9730.2010.00584.x.

Herrick, J.E., Lessard, V.C., Spaeth, K.E., Shaver, P.L., Dayton, R.S., Pyke, D.A., Jolley, L., Goebel, J.J., 2010. National ecosystem assessments supported by scientific and local knowledge. Frontiers in Ecology and Environment 8 (8), 403–408. http://dx.doi.org/10.1890/100017.

James, L.A., Watson, D.G., Hansen, W.F., 2007. Using LiDAR data to map gullies and headwater streams under forest canopy: South Carolina, USA. Catena 71 (1), 132–144. http://dx.doi.org/10.1016/j.catena.2006.10.010.

Jensen, J.R., 2005. Introductory digital imagery processing. 3rd ed. Pearson Prentice Hall, Upper Saddle River, NJ, USA, p. 526.

Karl, J.W., Duniway, M.C., Schrader, T.S., 2012. A technique for estimating rangeland canopy-gap size distributions from very-high-resolution digital imagery. Rangeland Ecology & Management 65 (2), 196–207. http://dx.doi.org/10.2111/rem-d-11-00006.1.

Kéfi, S., Alados, C.L., Chaves, R.C.G., Pueyo, Y., Rietkerk, M., 2010. Is the patch size distribution of vegetation a suitable indicator of desertification processes? Comment. Ecology 91, 3739–3742. http://dx.doi.org/10.1890/09-1915.1.

Korpela, I., 2006. Geometrically accurate time series of archived aerial images and airborne LiDAR data in a forest environment. Silva Fennica 40 (1), 109–126.

Lane, S.N., Westaway, R.M., Hicks, D.M., 2003. Estimation of erosion and deposition volumes in a large, gravel-bade, braided river using synoptic remote sensing. Earth Surface Processes and Landforms 28 (3), 249–271. http://dx.doi.org/10.1002/esp.483.

Loughran, R.J., 1989. The measurement of soil erosion. Progress in Physical Goegraphy 13, 216–233. http://dx.doi.org/10.1177/030913338901300203.

Lucieer, A., de long, S.M., Turner, D., 2013. Mapping landslide displacements using structure from motion (SfM) and image correlation of multi-temporal UAV photography. Progress in Physical Geography 38 (1), 97–116. http://dx.doi.org/10.1177/0309133313515293.

Martínez-Casasnovas, J.A., Ramos, M.C., Ribes-Dasi, M., 2002. Soil erosion caused by extreme rainfall events: mapping and quantification in agricultural plots from very detailed digital elevation models. Geoderma 105, 125–140. http://dx.doi.org/10.1016/s0016-7061(01)00096-9.

Martínez-Casasnovas, J.A., Anton-Fernandez, C., Ramos, M.C., 2003. Sediment production in large gullies of the Mediterranean area (NE Spain) from high-resolution digital elevation models and geographical information systems analysis. Earth Surface Processes and Landforms 28, 443–456. http://dx.doi.org/10.1002/esp.451.

Martínez-Casasnovas, J.A., 2003. A spatial information technology approach for the mapping and quantification of gully erosion. Catena 50, 293–308. http://dx.doi.org/10.1016/s0341-8162(02)00134-0.

Marzolff, I., Poesen, J., 2009. The potential of 3D gully monitoring with GIS using high-resolution aerial photography and a digital photogrammetry system. Geomorphology 111, 48–60. http://dx.doi.org/10.1016/j.geomorph.2008.05.047.

Marzolff, I., Ries, J.B., Poesen, J., 2011. Short-term versus medium-term monitoring for detecting gully-erosion variability in a Mediterranean environment. Earth Surface Processes and Landforms 36, 1604–1623. http://dx.doi.org/10.1002/esp.2172.

McGlone, J.C., 2013. Manual of photogrammetry. 6th ed. American Society for Photogrammetry and Remote Sensing, Bethesda, MD, USA, p. 1372.

Milan, D.J., Heritage, G.L., Large, A.R.G., Fuller, I.C., 2011. Filtering spatial error from DEMs: implications for morphological change estimation. Geomorphology 125, 160–171. http://dx.doi.org/10.1016/j.geomorph.2010.09.012.

Moffitt, F.H., Mikhail, E., 1980. Photogrammetry. 3rd ed. Harper & Row Publishers, New York, NY, USA, p. 648.

Mondino, E.B., Chiabrando, R., 2008. Multi-temporal block adjustment for aerial image time series: the Belvedere Glacier case study. The International Archives of the Photogrammetry, Remote Sensing and Spatial Information Sciences Beijing 37 (B2).

Mostafa, M., Hutton, J., 2001. Direct positioning and orientation systems. How do they work? What is the attainable accuracy? Proceedings, American Society of Photogrammetry and Remote Sensing Annual Meeting, St. Louis, MO, USA: American Society of Photogrammetry and Remote Sensing

Mostafa, M., Hutton, J., Lithopoulos, E., 2001. Airborne direct georeferencing of frame imagery: an error budget. The Third International Symposium on Mobile Mapping Technology, Cairo, Egypt.

National Research Council, 1994. Rangeland health: new methods to classify, inventory, and monitor rangelands. National Academy Press, Washington, DC, USA Available at: http://www.nap.edu/openbook.php?record_id=2212 Accessed April 10, 2014.

Nearing, M.A., Kimoto, A., Nichols, M.H., 2005. Spatial patterns of soil erosion and deposition in two small, semi-arid watersheds. Journal of Geophysical Research 110, F04020. http://dx.doi.org/10.1029/2005JF000290.

Nearing, M.A., Wei, H., Stone, J.J., Pierson, F.B., Spaeth, K.E., Weltz, M.A., Flanagan, D.C., Hernandez, M., 2011. A rangeland hydrology and erosion model. Transactions of the American Society of Agricultural and Biological Engineers 54 (3). http://dx.doi.org/10.13031/2013.37115.

Nichols, M.H., 2006. Measured sediment yield rates from semiarid rangeland watersheds. Rangeland Ecology & Management 59 (1), 55–62. http://dx.doi.org/10.2111/05-075r1.1.

Nouwakpo, S.K., Huang, C.H., 2012. A simplified close-range photogrammetric technique for soil erosion assessment. Soil Science Society of America Journal 76 (1), 70–84. http://dx.doi.org/10.2136/sssaj2011.0148.

Nusser, S.M., Goebel, J.J., 1997. The National Resources Inventory: a long-term multi-resource monitoring programme. Environmental and Ecological Statistics 4 (3), 181–204. http://dx.doi.org/10.1023/A:1018574412308.

Okin, G.S., 2008. A new model of wind erosion in the presence of vegetation. Journal of Geophysical Research: Earth Surface (2003–2012) 113 (F2). http://dx.doi.org/10.1029/2007jf000758.

Painter, T.H., Deems, J.S., Belnap, J., Hamlet, A.F., Landry, C.C., Udall, B., 2010. Response of Colorado River runoff to dust radiative forcing in snow. Proceedings of the National Academy of Sciences 107, 17125–17130. http://dx.doi.org/10.1073/pnas.0913139107.

Pellant, M., Shaver, P., Spaeth, K., 1999. Field test of a prototype rangeland inventory procedure in the western USA. In: Eldridge, D., Freudenberger, D. (Eds.), People and rangelands: building the future. Aitkenvale, Queensland 4814, Australia: Proceedings, VI International Rangeland Congress, p. 1072.

Perroy, R.L., Bookhagen, B., Asner, G.P., Chadwick, O.A., 2010. Comparison of gully erosion estimates using airborne and ground-based LiDAR on Santa Cruz Island, California. Geomorphology 118 (3–4), 288–300. http://dx.doi.org/10.1016/j.geomorph.2010.01.009.

Peters, D.P.C., Pielke, R.A., Bestelmeyer, B.T., Allen, C.D., Munson-McGee, S., Havstad, K.M., 2004. Cross-scale interactions, nonlinearities, and forecasting catastrophic events. Proceedings of the National Academy of Sciences of the United States of America 101, 15130–15135. http://dx.doi.org/10.1073/pnas.0403822101.

Peters, D.P.C., Sala, O.E., Allen, C.D., Covich, A., Brunson, M.W., 2007. Cascading events in linked ecological and socioeconomic systems. Frontiers of Ecology and the Environment 5, 221–224. http://dx.doi.org/10.1890/1540-9295(2007)5[221:CEILEA]2.0.CO;2.

Pimentel, D., Harvey, C., Resosudarmo, P., Sinclair, K., Kurz, D., McNair, M., Crist, S., Shpritz, L., Fitton, L., Saffouri, R., Blair, R., 1995. Environmental and economic costs of soil erosion and conservation benefits. Science 267 (5201), 1117–1123. http://dx.doi.org/10.1126/science.267.5201.1117.

Pimentel, D., Kounang, N., 1998. Ecology of soil erosion in ecosystems. Ecosystems 1, 416–426. http://dx.doi.org/10.1007/s100219900035.
Pyke, D.A., Herrick, J.E., Shaver, P., Pellant, M., 2002. Rangeland health attributes and indicators for qualitative assessment. Journal of Range Management 55, 584–597. http://dx.doi.org/10.2307/4004002.
PRISM Climate Group, 2013. PRISM climate dataAvailable at: http://www.prism.oregonstate.edu Accessed 22 March, 2013.
Rango, A., Laliberte, A., Herrick, J.E., Winters, C., Havstad, K., Steele, C., Browning, D., 2009. Unmanned aerial vehicle-based sensing for rangeland assessment, monitoring, and management. Journal of Applied Remote Sensing 3 (1), 033542. http://dx.doi.org/10.1117/1.3216822.
Reutebuch, S.E., McGaughey, R.J., Andersen, H.E., Carson, W.W., 2003. Accuracy of a high-resolution LiDAR terrain model under a conifer forest canopy. Canadian Journal of Remote Sensing 29 (5), 527–535. http://dx.doi.org/10.5589/m03-022.
Ritchie, J.C., McHenry, J.R., 1990. Applications of radioactive fallout cesium-137 for measuring soil erosion and sediment accumulation rates and patterns: a review. Journal of Environmental Quality 19, 215–233. http://dx.doi.org/10.2134/jeq1990.00472425001900020006x.
Robichaud, P.R., 2005. Measurement of post-fire hillslope erosion to evaluate and model rehabilitation treatment effectiveness and recovery. International Journal of Wildland Fire 14 (4), 475–485. http://dx.doi.org/10.1071/wf05031.
Robichaud, P.R., Wagenbrenner, J.W., Lewis, S.A., Ashmun, L.E., Brown, R.E., Wohlgemuth, P.M., 2013. Post-fire mulching for runoff and erosion mitigation Part II: Effectiveness in reducing runoff and sediment yields from small catchments. Catena 105, 93–111. http://dx.doi.org/10.1016/j.catena.2012.11.016.
Schlesinger, W.H., Reynolds, J.F., Cunningham, G.L., Huenneke, L.F., Jarrell, W.M., Virginia, R.A., Whitfor, W.G., 1990. Biological feedbacks in global desertification. Science 47 (4946), 1043–1048. http://dx.doi.org/10.1126/science.247.4946.1043.
Schneider, A., Gerke, H.H., Maurer, T., 2011. 3D initial sediment distribution and quantification of mass balances of an artificially-created hydrological catchment based on DEMs from aerial photographs using GOCAD. Physics and Chemistry of the Earth, Parts A/B/C 36, 87–100. http://dx.doi.org/10.1016/j.pce.2010.03.023.
Schneider, A., Gerke, H.H., Maurer, T., Seifert, S., Nenov, R., Huttl, R.F., 2012. Evaluation of remotely-sensed DEMs and modifications based on plausibility rules and initial sediment budgets of an artificially-created catchment. Earth Surface Processes and Landforms 37, 708–725. http://dx.doi.org/10.1002/esp.2274.
Shakesby, R.A., 1993. The soil erosion bridge; a devise for micro-profiling soil surface. Earth Surface Process and Landforms 18, 823–827. http://dx.doi.org/10.1002/esp.3290180906.
Skaloud, J., 2007. Reliability of direct georeferencing–beyond the Achilles' heel of modern airborne mapping. Photogrammetric Week 2007, 227–241.
Sirvent, J., Desir, G., Gutierrez, M., Sancho, C., Benito, G., 1997. Erosion rates in badland areas recorded by collectors, erosion pins, and profilometer techniques (Ebro Basin, NE-Spain). Geomorphology 18, 61–75. http://dx.doi.org/10.1016/s0169-555x(96)00023-2.
Smith, L.C., Alsdorf, D.E., Magilligan, F.J., Gomez, B., Mertes, L.A.K., Smith, N.D., Garvin, J.B., 2000. Estimation of erosion, deposition, and net volumetric change caused by the 1996 Skeiðarársandur jökulhlaup, Iceland, from Synthetic Aperture Radar Interferometry. Water Resources Research 36 (6), 1583–1594.
Thoma, D.P., Gupta, S.C., Bauer, M.E., Kirchoff, C.E., 2005. Airborne laser scanning for riverbank erosion assessment. Remote Sensing of the Environment 95 (4), 493–501. http://dx.doi.org/10.1016/j.rse.2005.01.012.
Thomas, A.W., Welch, R., Jordan, T.R., 1986. Quantifying concentrated-flow erosion on cropland with aerial photogrammetry. Journal of Soil and Water Conservation 41, 249–252.
Toevs, G.R., Karl, J.W., Taylor, J.J., Spurrier, C.S., Karl, M.S., Bobo, M.R., Herrick, J.E., 2011. Consistent indicators and methods and a scalable sample design to meet assessment, inventory, and monitoring information needs across scales. Rangelands 33 (4), 14–20. http://dx.doi.org/10.2111/1551-501x-33.4.14.
USDA (US Department of Agriculture), 2010. 2007 National Resources Inventory, Rangeland Resource Assessment. http://www.nrcs.usda.gov/Internet/FSE_DOCUMENTS/stelprdb1041707.pdf Accessed December 12, 2013.
US Geological SurveyAvailable at: http://gec.cr.usgs.gov/projects/sw/clim-met/dugout.html [Accessed 25 April, 2014].
USDA. Soil Conservation Service, 1991. Soil survey of Canyonlands Area, Utah, parts of Grand and San Juan Counties. Washington, DC. p. 293.
Vandaele, K., Vanommeslaeghe, J., Muylaert, R., Govers, G., 1996. Monitoring soil redistribution patterns using sequential aerial photographs. Earth Surface Processes and Landforms 21, 353–364. http://dx.doi.org/10.1002/(sici)1096-9837(199604)21:4<353::aid-esp568>3.0.co;2-8.
Welch, R., Jordan, T.R., Thomas, A.W., 1984. A photogrammetric technique for measuring soil erosion. Journal of Soil and Water Conservation 39, 191–194.
Westoby, M.J., Brasington, J., Glasser, N.F., Hambrey, M.J., Reynolds, J.M., 2012. 'Structure-from-Motion' photogrammetry: a low-cost, effective tool for geoscience applications. Geomorphology 179, 300–314. http://dx.doi.org/10.1016/j.geomorph.2012.08.021.
Wheaton, J.M., Brasington, J., Darby, S.E., Sear, D.A., 2010. Accounting for uncertainty in DEMs from repeat topographic surveys: improved sediment budgets. Earth Surface Processes and Landforms 35, 136–156. http://dx.doi.org/10.1002/esp.1886.
Wilcox, B.P., Pitlick, J., Allen, C.D., Davenport, D.W., 1996. Runoff and erosion from a rapidly eroding pinyon-juniper hillslope. In: Anderson, M.G., Brooks, S.M. (Eds.), Advances in hillslope processes. John Wiley & Sons, New York, NY, USA, pp. 61–71.
Wilson, S.J., Cooke, R.U., 1980. Wind erosion. In: Kirkby, M.J., Morgan, R.P.C. (Eds.), Soil erosion. Wiley, Chichester, England, pp. 217–251.
Wolf, P.R., Dewitt, B.A., 2000. Elements of photogrammetry: with applications in GIS. The McGraw-Hill Companies, Inc., New York, NY, USA, p. 624.
Yang, B., Chen, C., 2015. Automatic registration of UAV-borne sequent images and LiDAR data. ISPRS Journal of Photogrammetry and Remote Sensing 101, 262–274. http://dx.doi.org/10.1016/j.isprsjprs.2014.12.025.
Zapata, F., 2003. The use of environmental radionuclides as tracers in soil erosion and sedimentation investigations: recent advances and future developments. Soil & Tillage Research 69, 3–13. http://dx.doi.org/10.1016/s0167-1987(02)00124-1.
Zhang, Y.-G., Nearing, M.A., Liu, B.Y., Van Pelt, R.S., Stone, J.J., Wei, H., Scott, R.L., 2011. Comparative rates of wind versus water erosion from a small semiarid watershed in southern Arizona, USA. Aeolian Research 3 (2), 197–204. http://dx.doi.org/10.1016/j.aeolia.2011.03.006.